

***FATIGUE AND FRACTURE ANALYSIS OF  
GRAPHENE AND CNT EPOXY NANOCOMPOSITES***



**Thesis submitted in partial fulfilment for  
the award of degree**

***Doctor of Philosophy***

*by*

**Anupam Tiwari**

**Department of Mechanical Engineering  
Indian Institute of Technology  
(Banaras Hindu University)  
Varanasi-221005**

**16131001**

**2023**



**INDIAN INSTITUTE OF TECHNOLOGY  
(BANARAS HINDU UNIVERSITY),  
VARANASI-221005**

---

---

## **CERTIFICATE**

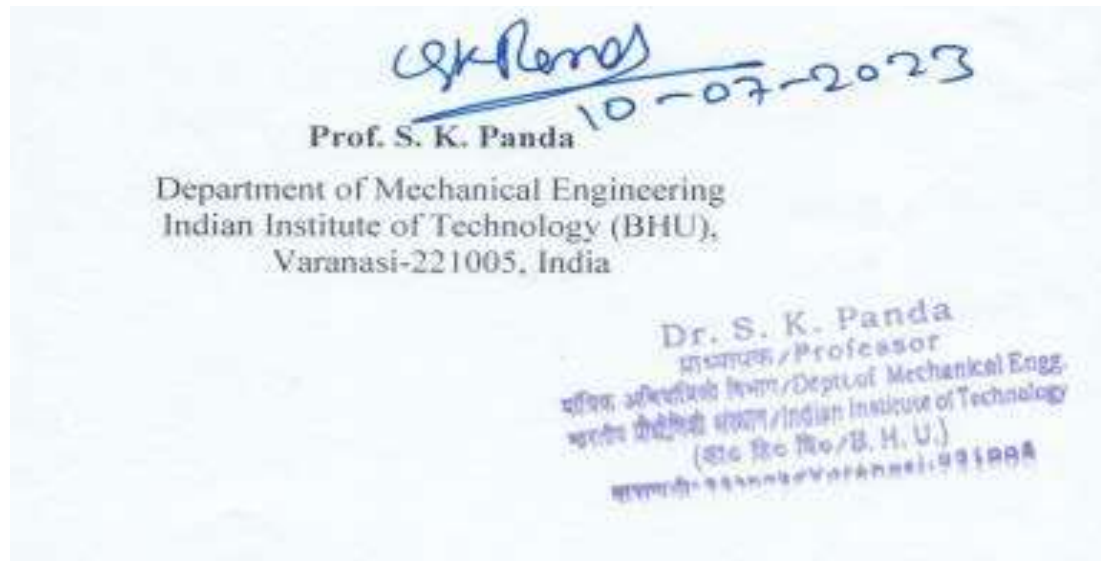
---

---

This is to certify that the work contained in the thesis titled "**FATIGUE AND FRACTURE ANALYSIS OF GRAPHENE AND CNT EPOXY NANOCOMPOSITES**" by "**ANUPAM TIWARI**" has been carried out under my/our supervision and that this work has not been submitted elsewhere for a degree.

It is further certified that the student has fulfilled all the requirements of Comprehensive Examination, Candidacy and SOTA for the award of Ph.D. Degree.

### **Supervisor**





INDIAN INSTITUTE OF TECHNOLOGY  
(BANARAS HINDU UNIVERSITY),  
VARANASI-221005

**DECLARATION BY THE CANDIDATE**

I "**Anupam Tiwari**", certify that the work embodied in this thesis is my own bona fide work and carried out by me under the supervision of "**Prof. S. K. Panda**" from "**July 2016 to July 2023**", at the "**DEPARTMENT OF MECHANICAL ENGINEERING**", Indian Institute of Technology (BHU), Varanasi. The matter embodied in this thesis has not been submitted for the award of any other degree/diploma.

I declare that I have faithfully acknowledged and given credits to the research workers wherever their works have been cited in my work in this thesis. I further declare that I have not willfully copied any other's work, paragraphs, text, data, results, *etc.*, reported in journals, books, magazines, reports dissertations, theses, *etc.*, or available at websites and have not included them in this thesis and have not cited as my own work

Date: 10/07/23

Place: Varanasi

Anupam Tiwari

Anupam Tiwari

**CERTIFICATE FROM THE SUPERVISOR**

This is to certify that the above statement made by the candidate is correct to the best of my knowledge

Prof. Santosh Kumar

Head of Department

Department of Mechanical Engineering,

Indian Institute of Technology (BHU),

Varanasi

विभागाध्यक्ष/HEAD

मैकैनिक्कल अभियान्तिकी विभाग/Deptt. of Mechanical Engg.

भारतीय प्रौद्योगिकी संस्थान/Indian Institute of

(काभं हिंदू विश्वविद्यालय/B.H.U.)

वाराणसी-221005/Varanasi-221005

Prof. S. K. Panda

Supervisor

Department of Mechanical Engineering

Indian Institute of Technology (BHU)

Varanasi

Dr. S. K. Panda

प्रभार/Professor

मैकैनिक्कल अभियान्तिकी विभाग/Deptt. of Mechanical Engg.

भारतीय प्रौद्योगिकी संस्थान/Indian Institute of Technology

(काभं हिंदू विश्वविद्यालय/B.H.U.)

वाराणसी-221005/Varanasi-221005



INDIAN INSTITUTE OF TECHNOLOGY  
(BANARAS HINDU UNIVERSITY),  
VARANASI-221005

---

---

## COPYRIGHT TRANSFER CERTIFICATE

---

---

**Title of the Thesis:** *FATIGUE AND FRACTURE ANALYSIS OF GRAPHENE  
AND CNT EPOXY NANOCOMPOSITES*

**Name of the Student:** ANUPAM TIWARI

---

---

### Copyright Transfer

---

---

The undersigned hereby assigns to the Indian Institute of Technology (Banaras Hindu University) Varanasi all rights under copyright that may exist in and for the above thesis submitted for the award of the "DOCTOR OF PHILOSOPHY".

Date: 10/07/23

Place: Varanasi

Anupam Tiwari

(ANUPAM TIWARI)

**Note:** However, the author may reproduce or authorize others to reproduce material extracted verbatim from the thesis or derivative of the thesis for author's personal use provided that the source and the Institute's copyright notice are indicated.

# ABSTRACT

---

---

Epoxy has been extensively studied for structural composites in industries such as aerospace, automotive, marine, construction, shipbuilding, and electronics. Its cross-linked structure imparts desirable properties like high glass transition temperature, stiffness, creep resistance, dimensional stability, and chemical resistance. However, uncured epoxy exhibits poor mechanical, chemical, and thermal properties. Curing with suitable agents forms a strong 3-D cross-linked structure but diminishes strength, fracture toughness, and fatigue resistance. Researchers have explored various nanoparticles and microparticles for reinforcement, with graphene nanoplatelets (GNP) emerging as superior nanofillers. Yet, challenges in exfoliation, dispersion, orientation, and interfacial bonding hinder graphene's full potential, thus limiting the structural applications of graphene-reinforced epoxy.

This study aimed to overcome challenges associated with the dispersion and spatial orientation of GNP to enhance the benefits of GNP epoxy nanocomposites. A mathematical model is developed to optimize the alignment parameters of GNP and magnetite ferric oxide ( $\text{Fe}_3\text{O}_4$ )-GNP applying a weak DC magnetic field (0.05T), considering rotation, translation, migration, and slackening mechanisms of the nanoparticle in the epoxy. Optimisation of magnetic field, epoxy viscosity, and time required to complete all mechanisms before gelation of epoxy has been carried out to fabricate a highly aligned GNP nanocomposite.

The characteristic magnetic, viscosity, and hydrodynamic parameters required by the mathematic model are determined experimentally. The  $\text{Fe}_3\text{O}_4$  synthesized by solve-thermal and attaching them to the GNP surface to increase its magnetic susceptibility in order to utilize the model's suggested optimized magnetic parameters. The Morphology, microstructure, and magnetic properties of GNP,  $\text{Fe}_3\text{O}_4$ , and  $\text{Fe}_3\text{O}_4$ -GNP nanoparticles have been characterized by

XRD, FTIR, Raman spectroscopy, TGA, AFM, XPS, BET, TEM, SEM, EDXMA, and VSM. A highly aligned Fe<sub>3</sub>O<sub>4</sub>-GNP nanocomposite is fabricated at 0.05T magnetic field and 40Pa-s dynamic viscosity of epoxy, as evident from the aforementioned characterization methods, DSC, optical microscopy, and studying the fracture surface morphology confirmed the highly aligned alignment Fe<sub>3</sub>O<sub>4</sub>-GNP epoxy nanocomposite.

Furthermore, our investigation focuses the influence and comparative impact of alignment, as well as wt% loading, of both nanoparticles GNP and Fe<sub>3</sub>O<sub>4</sub>-GNP on various mechanical properties, such as tensile and compressive strength,  $K_{IC}$ ,  $G_{IC}$ ,  $CTOD_c$ , crack propagation, and fracture mechanisms. This study utilizes AFM analysis to examine the roughness parameters of fractured surfaces. The conclusion asserts that nanoparticle alignment increases the likelihood of primary crack fronts interaction and results in a change in a stress state, deflection, branching, and bifurcation, ultimately leading to increased crack growth resistance.

Moreover, being a leading cause of catastrophic failure in structural materials, fatigue is the primary focus of this present study, which aims to investigate the fatigue thresholds ( $\Delta K_{th}$  and  $\Delta G_{th}$ ) fatigue crack growth rate (FCGR) resistance, and the contribution of toughening mechanisms under cyclic fatigue loading in the nanocomposites. The investigation concludes that increasing the weight percentage (wt%) leads to higher  $\Delta K_{th}$ ,  $\Delta G_{th}$  and FCGR resistance, with alignment having a more significant impact. Moreover, the Paris law constants ( $C$ ,  $C'$ , and  $m$ ) exhibit a decrease. Through fractography and roughness analysis, it has been determined that alignment enhances the probability of interaction among primary crack fronts, leading to tip shielding, crack bifurcation, deflection, local mixed mode, striation marks, shear yielding, crack twisting and tilting, micro-crazing, void nucleation, nanoparticle debonding, pullout, and cavitation. Consequently, the alignment significantly enhances resistance to FCGR.

As part of this Ph.D. study, we also investigated the fracture energy of CNT/epoxy nanocomposites using a mathematical model. The characteristics of the debonding process zone

involving macro-scale, micro-scale and nano-scale mechanisms along CNT interface influence the fracture behaviour of nanocomposites and their structural integrity. In current study, a multi-scale and multi-mechanism modelling approach with a cylindrical RVE comprising CNT, interphase and matrix is developed to assess such damage progression and energy dissipation occurring at the nano-scale. The model considers the dominant damaging phenomena emerging in CNT/epoxy nanocomposites, i.e., CNT debonding with an interphase zone around nanoparticles, cavitation, and plastic deformation of nanovoids. Enhancement of fracture toughness with the weight fraction of CNT is investigated with a qualitative variation of geometric and mechanical properties of the interphase, cavitation and plastic yielding adopting strain energy release rate procedures. The fracture energy is shown to be critically influenced by the stiffness ratio of interphase to the matrix, interphase thickness, and hardening exponent. The Model is validated using experimental and analytical data.

## **DEDICATION**

I dedicate this thesis to **Shri Vishwanath Temple (VT), BHU**, the eternal source of inspiration and wisdom, guiding my academic journey beyond earthly bounds. Its cosmic presence symbolizes knowledge's eternal cycle, providing unwavering strength and insight for my quest.

## **ACKNOWLEDGEMENTS**

---

---

I would like to start by expressing my gratitude to the divine power, God, for guiding me into this realm of intellectual pursuit.

First and foremost, I extend my deepest appreciation to my esteemed mentors, Prof. S. K. Panda, for their unwavering support, encouragement, and enlightening discussions throughout my research. Their involvement and tireless efforts have been invaluable, and I am truly indebted to them for their motivation and emphasis on persistent commitment. Completing this thesis would have been impossible without their guidance.

Additionally, I am grateful to my RPEC members, Dr. Amit Tyagi of Department of Mechanical Engineering and Dr. M. R. Majhi of Ceramic Engineering, for their valuable feedback and encouragement. I sincerely thank the Heads of the Department of Mechanical Engineering, both past and present, for providing the necessary research facilities that enabled the successful completion of my work. The cooperation and support from the faculty members, staff, and workshop at IIT (BHU), Varanasi have been invaluable, and I deeply appreciate their assistance. I would also like to extend my gratitude to the Convener DPGC and all esteemed DPGC members for their kind support.

Furthermore, I am grateful to my seniors, juniors, colleagues, and friends for engaging in fruitful discussions and continuously encouraging me throughout my time at IIT (BHU), Varanasi.

Last but not the least, I express my utmost gratitude to my parents, uncle, aunt, and all my family members for their unwavering support and encouragement throughout this journey.

**Anupam Tiwari**

# Contents

<i>CERTIFICATE</i> .....	<i>ii</i>
<i>DECLARATION BY THE CANDIDATE</i> .....	<i>iii</i>
<i>CERTIFICATE FROM THE SUPERVISOR</i> .....	<i>iii</i>
<i>COPYRIGHT TRANSFER CERTIFICATE</i> .....	<i>iv</i>
<i>ABSTRACT</i> .....	<i>v</i>
<i>DEDICATION</i> .....	<i>viii</i>
<i>ACKNOWLEDGEMENTS</i> .....	<i>ix</i>
<i>Contents</i> .....	<i>x</i>
<i>List of Figures</i> .....	<i>xvii</i>
<i>List of Tables</i> .....	<i>xxii</i>
<i>List of Abbreviations</i> .....	<i>xxiii</i>
<i>List of Nomenclature</i> .....	<i>xxv</i>
<i>Preface</i> .....	<i>xxviii</i>
<b>Chapter 1. Introduction</b> .....	<b>1</b>
1.1. Background.....	1
1.1.1. FRP Composites .....	2
1.1.2. Nanocomposite .....	3
1.2. Motivation .....	8
<b>Chapter 2. Literature Review</b> .....	<b>13</b>
2.1. Introduction .....	13

2.2.	Epoxy.....	13
2.3.	Nanoparticles Reinforcement .....	17
2.3.1.	Metal-based nanoparticles .....	18
2.3.2.	Clay nanoparticles.....	18
2.3.3.	Ceramic nanoparticles.....	19
2.3.4.	Polymer-based nanoparticles .....	19
2.3.5.	Carbon-based nanoparticles .....	20
2.4.	Graphene.....	20
2.5.	CNT .....	22
2.6.	Fabrication of GNP and CNT epoxy nanocomposite.....	26
2.7.	Research Gap.....	27
2.8.	Research Aims and Objectives .....	30
2.9.	Structure of The Thesis.....	31

**Chapter 3. Development of Nanocomposite by Magnetic Field Induced Alignment of GNP**

**35**

3.1.	Introduction .....	35
3.2.	Method: Physical phenomena of applied DC electromagnetic-coerced alignment of Fe <sub>3</sub> O <sub>4</sub> -GNP .....	35
3.2.1.	Rotation of Fe <sub>3</sub> O <sub>4</sub> -GNP particles .....	39
3.2.2.	Chaining of Fe <sub>3</sub> O <sub>4</sub> -GNP nanoparticles.....	42
3.2.3.	Migration of Fe <sub>3</sub> O <sub>4</sub> -GNP nanoparticles .....	47
3.2.4.	Slackening of aligned Fe <sub>3</sub> O <sub>4</sub> -GNP nanoparticles.....	48
3.3.	Experimental section .....	49
3.4.	Results and discussion.....	50

3.4.1.	Experimental results .....	50
3.5.	Model Results .....	52
3.5.1.	Rotation.....	53
3.5.2.	Chaining of nanoparticles .....	55
3.5.3.	Migration .....	57
3.5.4.	Slackening.....	58
3.5.5.	Considerations on the model results .....	58
3.6.	Conclusion .....	60
<b>Chapter 4. Experimental Characterization Optimising Alignment Parameters of GNP Epoxy Base nanocomposite.....</b>		<b>62</b>
4.1.	Introduction .....	62
4.2.	Experimental section .....	62
4.2.1.	Basic materials.....	63
4.2.2.	Synthesis of Fe <sub>3</sub> O <sub>4</sub> and Fe <sub>3</sub> O <sub>4</sub> -GNP.....	63
4.2.3.	Preparation of GNP epoxy and Fe <sub>3</sub> O <sub>4</sub> -GNP epoxy nanocomposites .....	64
4.3.	Characterization, morphology and microstructure of GNP, Fe <sub>3</sub> O <sub>4</sub> -GNP and nanocomposites .....	68
4.3.1.	HR-XRD (High Resolution X-Ray Diffraction).....	68
4.3.2.	FTIR (Fourier transform infrared spectroscopy).....	68
4.3.3.	Raman measurements .....	68
4.3.4.	TGA (Thermogravimetric analysis).....	69
4.3.5.	DSC (Differential scanning calorimetry).....	69
4.3.6.	AFM (Atomic force microscopy) .....	69
4.3.7.	XPS (X-ray photoelectron spectroscopy analysis).....	69
4.3.8.	BET (Brunauer–Emmett–Teller) analysis.....	70
4.3.9.	Exploration of the alignment of the Fe <sub>3</sub> O <sub>4</sub> -GNP.....	70
4.3.10.	HR-SEM and HR-TEM analysis .....	70

4.3.11.	Chemorheological behaviours of epoxy during curing .....	70
4.3.12.	Measurement of magnetic properties .....	71
4.4.	Results and discussion .....	71
4.4.1.	HR-XRD analysis .....	71
4.4.2.	FTIR (Fourier transform infrared spectroscopy).....	74
4.4.3.	Raman spectroscopy .....	74
4.4.4.	TGA (Thermogravimetric analysis).....	75
4.4.5.	DSC (Differential scanning calorimetry).....	77
4.4.6.	XPS (X-ray photoelectron spectroscopy analysis).....	79
4.4.7.	BET (Brunauer–Emmett–Teller) analysis.....	81
4.4.8.	Exploration of the alignment of the Fe <sub>3</sub> O <sub>4</sub> -GNP.....	82
4.4.9.	SEM and TEM analysis .....	82
4.4.10.	AFM analysis .....	86
4.4.11.	Magnetic properties of GNP, Fe <sub>3</sub> O <sub>4</sub> , and Fe <sub>3</sub> O <sub>4</sub> -GNP .....	90
4.4.12.	Chemorheological behaviour of epoxy during curing.....	91
4.5.	Conclusion .....	92
<b>Chapter 5. Fracture and Failure Analysis of GNP and Aligned Fe<sub>3</sub>O<sub>4</sub>-GNP Epoxy Nanocomposite .....</b>		
<b>94</b>		
5.1.	Introduction .....	94
5.2.	Experimental.....	95
5.2.1.	Basic Materials .....	95
5.2.2.	Preparation of GNP epoxy and aligned Fe <sub>3</sub> O <sub>4</sub> -GNP epoxy nanocomposites.....	95
5.3.	Mechanical properties.....	95
5.3.1.	Tensile tests .....	95
5.3.2.	Compression tests .....	96
5.3.3.	Compact tension (CT) test for fracture toughness .....	96
5.3.4.	CTOD <sub>c</sub> measurement by clip gauges .....	99

5.3.5.	Fracture surface analysis.....	100
5.4.	Results .....	102
5.4.1.	Tensile Properties .....	102
5.4.1.1.	Maximum tensile load.....	104
5.4.1.2.	Maximum tensile extension.....	105
5.4.1.3.	Young's modulus.....	106
5.4.1.4.	Yield strength .....	107
5.4.1.5.	Toughness.....	108
5.4.2.	Compression Properties .....	109
5.4.2.1.	Compressive yield strength .....	110
5.4.2.2.	Compressive modulus .....	112
5.4.3.	Fracture toughness and fracture energy .....	114
5.4.3.1.	Maximum CT load .....	115
5.4.3.2.	Stress intensity factor .....	116
5.4.3.3.	Strain energy release rate.....	118
5.4.3.4.	Critical Crack Tip opening displacement .....	119
5.4.4.	Fracture surface analysis.....	122
5.4.4.1.	Stereo zoom optical microscopy.....	122
5.4.4.2.	Atomic force microscopy .....	123
5.5.	Discussion.....	130
5.6.	Conclusions .....	135
<b>Chapter 6. Fatigue Analysis of GNP and Aligned Fe<sub>3</sub>O<sub>4</sub>-GNP Epoxy Nanocomposite. 136</b>		
6.1.	Introduction .....	136
6.2.	Experimental procedure.....	137
6.2.1.	Materials and specimen preparation the nanocomposites .....	137
6.2.2.	Cyclic fatigue and FCGR test .....	138
6.2.3.	Fatigue fracture surface analysis.....	142

6.3.	Result .....	142
6.3.1.	Cyclic fatigue loading and its response.....	143
6.3.2.	The impact of nanoparticles on thresholds for fatigue crack growth, $\Delta K_{th}$ and $\Delta G_{th}$ .....	147
6.3.3.	The influence of nanoparticles on the FCGR.....	150
6.3.4.	The impact of nanoparticles on the constant of the Paris law .....	153
6.3.5.	Fatigue fracture surface analysis.....	158
6.4.	Discussion.....	163
6.4.1.	Thermal softening.....	164
6.4.2.	Fatigue crack growth mechanism .....	165
6.5.	Conclusion.....	168
<b>Chapter 7. Fracture Energy of CNT/Epoxy Nanocomposites with Progressive Interphase Debonding, Cavitation, and Plastic Deformation of Nanovoids .....</b>		<b>170</b>
7.1.	Introduction .....	170
7.2.	A theoretical multi-scale modelling approach.....	171
7.2.1.	General concepts.....	171
7.2.1.1.	Macro-scale: .....	172
7.2.1.2.	Micro-scale:.....	173
7.2.1.3.	Nano-scale:.....	173
7.2.2.	Mean mechanical properties and stiffness tensor.....	173
7.2.3.	Description of RVE .....	174
7.3.	Energy release rate procedure in multi-scale modelling .....	177
7.4.	Elastic debonding induced toughness improvement .....	183
7.5.	Cavitation.....	185
7.6.	Plastic deformation of nanovoids .....	186
7.7.	Results and discussion .....	191

7.7.1.	Effect of the interphase properties on cavitation-induced toughness improvement.....	192
7.7.2.	Growth of nanovoid and plastic deformation.....	192
7.7.3.	Experimental comparison of fracture energy, analytical evaluation and error.....	194
7.8.	Conclusions .....	199
	Supplementary .....	200
<b>Chapter 8. Conclusion and Future Scope .....</b>		<b>202</b>
8.1.	Introduction .....	202
8.2.	Conclusion .....	202
8.2.1.	Development of nanocomposite by Magnetic Field Induced Alignment of Graphene Nanoplatelets 203	
8.2.2.	Experimental Characterization Optimising Alignment Parameters of GNP epoxy base nanocomposite.....	203
8.2.3.	Fracture and Failure Analysis of GNP and aligned Fe <sub>3</sub> O <sub>4</sub> -GNP epoxy Nanocomposite .....	204
8.2.4.	Fatigue Analysis of GNP and aligned Fe <sub>3</sub> O <sub>4</sub> -GNP epoxy Nanocomposite.....	205
8.2.5.	Fracture Energy of CNT/Epoxy Nanocomposites with Progressive Interphase Debonding, Cavitation, and Plastic Deformation of Nanovoids .....	206
8.3.	Future Scope .....	208
<b>REFERENCES .....</b>		<b>210</b>
<b>List of Publications.....</b>		<b>232</b>

## List of Figures

Fig. 1.1 Shows the example of FRP composite (source Internet) .....	4
Fig. 1.2 Depicts the example of nanocomposites[73] .....	5
Fig. 1.3 Shows components made of FRP composite used in Airbus[283] .....	6
Fig. 1.4 Shows components made of nanocomposite used in Aerospace [284]. .....	7
Fig. 2.1 Define the families of polymer (source internet) .....	15
Fig. 2.2 Demonstrate the chemical structure formula of LY-556 and HY-951 .....	16
Fig. 2.3. Mother of all graphitic forms. Graphene is a 2D building material for carbon materials of all other dimensionalities. It can be wrapped up into 0D buckyballs, rolled into 1D nanotubes or stacked into 3D graphite. (Reproduced with permission from ref. [45]. Copyright 2016 Springer Publications). .....	25
Fig. 3.1. Shows the schematic illustration of graphene nanoplatelets (GNP) and functionalized GNP with magnetic nanoparticles Fe <sub>3</sub> O <sub>4</sub> i.e., Fe <sub>3</sub> O <sub>4</sub> -GNP .....	37
Fig. 3.2. Visualizes the Fe <sub>3</sub> O <sub>4</sub> -GNP as the shape of an oblate spheroid and also denotes equatorial radius ‘ <i>a</i> ’ as well as the distance ‘ <i>b</i> ’ from the centre to pole along the symmetry axis of the Fe <sub>3</sub> O <sub>4</sub> -GNP. ....	37
Fig. 3.3. Displays the angle ‘ <i>θ</i> ’ between the direction of applied magnetic field ‘ <i>H<sub>0</sub></i> ’ and easy axis of Fe <sub>3</sub> O <sub>4</sub> -GNP as well as the induced magnetic torque about x-axis ‘ <i>T<sub>xm</sub></i> ’ on the dispersed Fe <sub>3</sub> O <sub>4</sub> -GNP in epoxy. ....	38
Fig. 3.4. Illustrates the orientation mechanism of the Fe <sub>3</sub> O <sub>4</sub> -GNP (a) Initiation of rotation. (b) Completion of rotation and initiation of chaining. (c) Completion of chaining and initiation of migration (d) Migration phenomena. ....	44
Fig. 3.5. Shows the schematic representation of the volume associated with a single Fe <sub>3</sub> O <sub>4</sub> -GNP nanoparticle after the orientation in the magnetic field direction. ....	46
Fig. 3.6. Illustrates the slackening of Fe <sub>3</sub> O <sub>4</sub> -GNP nanoparticles after removal of magnetic fields. ....	48
Fig. 3.7. Shows chemorheological behaviours of Epoxy LY-556 and Hardener HY-951 with ratio 10:1 during curing process.....	51
Fig. 3.8. show the optical microscope images of the Fe <sub>3</sub> O <sub>4</sub> -GNP before and after curing in the epoxy under the weak magnetic field.....	52
Fig. 3.9. Shows the (a) saturation magnetization ( <i>M<sub>S</sub></i> ) vs. applied Magnetic field ( <i>H<sub>0</sub></i> ) having details the characteristics of coercivity and remanence, while (b) demonstrates the mass magnetic susceptibility( <i>χ</i> ) vs. applied magnetic field ( <i>H<sub>0</sub></i> ) of Fe <sub>3</sub> O <sub>4</sub> -GNP.....	52
Fig. 3.10. Shows the plots of the alignment time of the (a) GNP and (b) Fe <sub>3</sub> O <sub>4</sub> -GNP as a function of the initial angle <i>θ<sup>0</sup></i> for the rotational motion.....	54
Fig. 3.11. shows the influence of the magnetic field and viscosity on the rotational time of (a) and (c) GNP, (b) and (d) Fe <sub>3</sub> O <sub>4</sub> -GNP.....	55
Fig. 3.12. shows the influence of the magnetic field and viscosity on the chaining time of (a) and (c) GNP, (b) and (d) Fe <sub>3</sub> O <sub>4</sub> -GNP.....	56

Fig. 3.13. demonstrates how the magnetic field and viscosity affect the migration time of (a) and (c) GNP, (b) and (d) Fe <sub>3</sub> O <sub>4</sub> -GNP.....	57
Fig. 3.14. shows the influence viscosity on the rotational and translation slackening time of (a) GNP and (b) Fe <sub>3</sub> O <sub>4</sub> -GNP. ....	58
Fig. 4.1. Shows the all steps during fabrication process of the GNP and FE3O4-GNP nanoparticle reinforced nanocomposites.....	66
Fig. 4.2. Schematically explain the mechanism of cross-linking reaction of (a) neat epoxy (b) GNP epoxy (c) Fe3O4-GNP epoxy fabrication (d) orientation of GNP and aligned Fe3O4-GNP in epoxy, while, (e) the significance of graphical notations. ....	67
Fig. 4.3. Shows the comparative X-ray diffraction of (a) GNP, Fe <sub>3</sub> O <sub>4</sub> , and Fe <sub>3</sub> O <sub>4</sub> -GNP and (b) epoxy, GNP epoxy and Fe <sub>3</sub> O <sub>4</sub> -GNP epoxy nanocomposites. ....	72
Fig. 4.4. Shows the comparative Fourier-transform infrared spectroscopic (FTIR) analysis of GNP, Fe <sub>3</sub> O <sub>4</sub> , and Fe <sub>3</sub> O <sub>4</sub> -GNP.....	73
Fig. 4.5. Shows the comparative Raman spectroscopic analysis of (a) GNP, Fe <sub>3</sub> O <sub>4</sub> , and Fe <sub>3</sub> O <sub>4</sub> -GNP; and (b) epoxy, GNP epoxy and Fe <sub>3</sub> O <sub>4</sub> -GNP epoxy. ....	77
Fig. 4.6. Describes the comparative thermogravimetric analysis (TGA) of (a) GNP, Fe <sub>3</sub> O <sub>4</sub> , Fe <sub>3</sub> O <sub>4</sub> -GNP and (b) their nanocomposites. ....	77
Fig 4.7. Explains the DSC thermograms of epoxy, GNP epoxy and aligned Fe3O4-GNP epoxy at constant heating rate 10°C/min. (a)The glass transition temperature (T <sub>g</sub> ) is mentioned with each thermograms and (b) Higher heating .....	78
Fig. 4.8 show (a) survey spectrum of the GNP and Fe <sub>3</sub> O <sub>4</sub> -GNP;(b) high resolution Fe2p scan of the Fe <sub>3</sub> O <sub>4</sub> -GNP; (c) and (d) High-resolution O1s scans of GNP and Fe <sub>3</sub> O <sub>4</sub> -GNP, respectively; and (d) and (f) high resolution C1s scans of GNPs and Fe <sub>3</sub> O <sub>4</sub> -GNP.....	80
Fig. 4.9. Shows (a) N <sub>2</sub> adsorption and desorption isotherms (b) BJH isotherm curves (by adsorption) (c) cumulated surface area vs. pore diameter and (d) cumulated pore volume vs. pore diameter of GNP and Fe <sub>3</sub> O <sub>4</sub> -GNP. ....	81
Fig. 4.10. Show (a) the surface morphology of the GNP, (b) a particle of the GNP, (c) the particles size distribution and (d) elemental analysis of the GNP.....	83
Fig. 4.11. Illustrate TEM of GNP and Fe <sub>3</sub> O <sub>4</sub> -GNP nanoparticles. (e) Fe <sub>3</sub> O <sub>4</sub> -GNP nanoparticles show that Fe <sub>3</sub> O <sub>4</sub> particles are attached on the GNP surfaces; (c) SAED pattern showing the nanoparticles structure, where the lattice planes of GNP and Fe <sub>3</sub> O <sub>4</sub> -GNP are clearly visible. ....	84
Fig. 4.12. Shows the (a), (c) and (d) SEM images of fracture surfaces and (b), (d), (f) the relative fracture surfaces nature. ....	85
Fig. 4.13. Shows (a) and (e) an illustration of nanoparticles deposition on a mica substrate captured using the standard AFM tapping mode, (b) and (f) particles size distribution, (c) and (g) 3D roughness of single surface, (d) and (h) surfaces texture of the GNP and Fe <sub>3</sub> O <sub>4</sub> -GNP, respectively.....	87
Fig. 4.14. Shows (a, c, e) the 3D roughness profile and (b, d, f) surface roughness parameters of the fracture surfaces of the nanocomposite.....	88
Fig. 4.15. Shows the Gaussian distribution of equatorial diameter of the GNP and Fe <sub>3</sub> O <sub>4</sub> -GNP measured by Dynamic light scattering. ....	89

Fig. 4.16. Shows the (a) saturation magnetization ( $M_S$ ) vs. applied Magnetic field ( $H_0$ ) having details the characteristics of coercivity and remanence, while (b) demonstrates the mass magnetic susceptibility( $\chi$ ) vs. applied magnetic field ( $H_0$ ) of $Fe_3O_4$ -GNP.....	91
Fig. 5.1. Displays(a) and (b) the experimental set up of tensile testing, (c) ASTM for the tensile (d), and final nanocomposite specimen. ....	98
Fig. 5.2. Shows the experimental set up of compressive test (a) and (b), ASTM for the test (c), and final compressive specimen (d) and (e).....	99
Fig. 5.3. Visualises the experimental set up, ASTM of fracture testing, and knife edge configuration at <i>COD</i> tips. ....	101
Fig. 5.4. Demonstrates the hypothetical crack opening configuration and growth phenomena under the Mode-I loading.....	102
Fig. 5.5. Indicates the engineering stress and engineering strain behaviour of the nanocomposites under tensile loading at crosshead rates of 1 mm/min and ambient conditions (30 °C, humidity 50%). ....	103
Fig. 5.6. Shows the maximum tensile load sustained by the nanocomposite under tensile loading with different nanoparticle weight percentages. The error bar represents the Standard Deviation of data.....	104
Fig. 5.7. Displays the maximum tensile extension sustained by the nanocomposite under tensile loading with different nanoparticle weight percentages. The error bar represents the Standard Deviation of data. ....	105
Fig. 5.8. Shows the Young's Modulus of the nanocomposite under tensile loading with different nanoparticle weight percentages. The error bar represents the Standard Deviation of data. ....	106
Fig. 5.9. Shows the Yield strength of the nanocomposite under tensile loading with different nanoparticle weight percentages. The error bar represents the Standard Deviation of data. ....	107
Fig. 5.10. Shows the toughness of the nanocomposite under tensile loading with different nanoparticle weight percentages. The error bar represents the Standard Deviation of data. ....	109
Fig. 5.11. Visualise the engineering compressive stress and engineering compressive strain behaviour of the nanocomposites under compressive loading at crosshead rates of 1 mm/min and ambient conditions (30 °C, humidity 50%).. ....	110
Fig. 5.12. Shows the compressive Yield strength of the nanocomposite under compressive loading with different nanoparticle weight percentages. The error bar represents the Standard Deviation of data.....	111
Fig. 5.13. Shows the compressive modulus of the nanocomposite under compressive loading with different nanoparticle weight percentages. The error bar represents the Standard Deviation of data. ....	113
Fig. 5.14. Indicates the load and crack opening displacement (COD) behaviour of the nanocomposites under compact tension test at crosshead rates of 0.1 mm/min and ambient conditions (30 °C, humidity 50%).....	114
Fig. 5.15. Shows the maximum load sustained by the nanocomposite under compact tension test with different nanoparticle weight percentages. The error bar represents the Standard	

Deviation of data. The dotted line indicates that a polynomial adequately fits the data, while $R^2$ determined the quality of fit. ....	115
Fig. 5.16. Shows the Stress intensity factor of the nanocomposite with different nanoparticle weight percentages. The error bar represents the Standard Deviation of data. The dotted line indicates that a polynomial adequately fits the data, while $R^2$ determined the quality of fit. ....	117
Fig. 5.17. Shows the Strain energy release rate of the nanocomposite with different nanoparticle weight percentages. The error bar represents the Standard Deviation of data. ....	118
Fig. 5.18. Displays the crack tip opening displacement of nanocomposite with different nanoparticle weight percentages during the fracture .....	120
Fig. 5.19. Displays the stress intensity factor of the nanocomposite at different Crack Tip opening displacement during the fracture. ....	121
Fig. 5.20. Display stereo-zoom microscopic images of the fractured surfaces of the nanocomposites at three different spots for neat epoxy, 0.300wt%, and 0.600wt% of both GNP and Aligned Fe <sub>3</sub> O <sub>4</sub> -GNP nanoparticles.....	123
Fig. 5.21. Demonstrates the Atomic Force Microscope for 3D roughness parameters of the fractured surfaces of the nanocomposites. ....	127
Fig. 5.22. Shows the roughness of the fracture surface of the nanocomposite with different nanoparticles. The error bar represents the Standard Deviation of data. ....	129
Fig. 5.23. Shows the roughness wavinessprofile of the fracture surface of the nanocomposite with different nanoparticles. ....	130
Fig. 6.1. Illustrates the experimental arrangement, with a CT specimen employed according to ASTM standards for fracture testing and also attachment of the COD to the CT specimen through the implementation of a knife-edge configuration.....	137
Fig. 6.2. Illustrates an algorithm flowchart that explicitly outlines each step involved in the computation of fatigue crack growth parameters. ....	141
Fig. 6.3. Illustrates the COD response under the applied sinusoidal load for a typical cycle of a nanocomposite. ....	145
Fig. 6.4. show the hysteresis loops showcasing the relationship between the applied sinusoidal Load and the corresponding COD response of typical a nanocomposite during two representative progressive cycles .....	147
Fig. 6.5. Illustrates the COD response under the applied sinusoidal load for a typical cycle of a nanocomposite. ....	148
Fig. 6.6. Elucidates the fatigue crack growth rate at a specific number of cycles and corresponding crack growth for a typical a nanocomposite under the applied sinusoidal load. ....	150
Fig. 6.7. Presents logarithmic plots (Log-Log) illustrating the correlation between the fatigue crack growth rate ( $dadN$ ) the stress intensity factor range ( $\Delta KI$ ) specifically for epoxy, GNP epoxy, and aligned Fe <sub>3</sub> O <sub>4</sub> -GNP epoxy nanocomposites. ....	153
Fig. 6.8. Depicts logarithmic plots (Log-Log) illustrating the correlation between the fatigue crack growth rate ( $dadN$ ) and the strain energy release rate ( $\Delta GI$ ) specifically for epoxy, GNP epoxy, and aligned Fe <sub>3</sub> O <sub>4</sub> -GNP epoxy nanocomposites .....	154

Fig. 6.9. Shows the influence of nanoparticles' wt% and the alignment of nanoparticles on the critical stress intensity factor ( $\Delta K_{th}$ ) specifically for epoxy, GNP epoxy, and aligned Fe <sub>3</sub> O <sub>4</sub> -GNP epoxy nanocomposites .....	155
Fig. 6.10. Shows the influence of nanoparticles' wt% and the alignment of nanoparticles on the critical strain energy release rate ( $\Delta G_{th}$ ) specifically for epoxy, GNP epoxy, and aligned Fe <sub>3</sub> O <sub>4</sub> -GNP epoxy nanocomposites and.....	156
Fig. 6.11. Showcases stereo-zoom optical microscopic images of the fractured surfaces caused by the fatigue crack growth in epoxy, GNP epoxy, and aligned Fe <sub>3</sub> O <sub>4</sub> -GNP nanoparticle nanocomposites (0.600wt%) at three distinct progressive locations, illustrative of the mechanisms involved in the fatigue crack growth.(Notion- <i>A: Alteration of plane</i> , <i>B: Bifurcation</i> , <i>C: Crack deflection</i> , <i>D:</i> , <i>I: Initiation of crack</i> , <i>M: local Mixed mode</i> , <i>R: River line</i> , <i>T:Twisting</i> , <i>Tl: Tilting</i> , <i>S: Striation marks</i> , <i>Sy: Shear yielding</i> .).....	160
Fig. 6.12. Investigates the atomic force microscopy images of the fractured surfaces near the crack initiation in (a) epoxy, (b) GNP epoxy, and (c) aligned Fe <sub>3</sub> O <sub>4</sub> -GNP epoxy nanocomposites during fatigue crack growth. Notably, the images in (c) demonstrate the alignment of Fe <sub>3</sub> O <sub>4</sub> -GNP nanoparticles, while (d) exhibits the wavy characteristics of the fractured surfaces, resembling the path of the crack. ....	163
Fig. 7.1 Correlation of macro, micro, and nanoscale stress system .....	172
Fig. 7.2. Illustration of multiscale system under analysis. ....	175
Fig. 7.3. Applied stresses on RVE and continuity conditions before and after debonding....	176
Fig. 7.4 Loading and Stress field near crack tip.....	182
Fig. 7.5. Normalized energy release rate enhancement due to cavitation; considering different (a) interphase thicknesses (t) and (b) interphase stiffness( $E_i = \lambda E_m$ ).....	196
Fig. 7.6. Normalized energy release rate enhancement due to plastic deformation of nanovoids; considering different (a) interphase stiffness( $E_i = \lambda E_m$ ), (b) hardening exponents (n) and (c) interphase thicknesses (t). ....	197

## List of Tables

---

---

Table 2.1 Key properties of the matrix and Curing agent .....	14
Table 2.2. A thorough review of articles investigating nanoparticle alignment methods utilizing various applied external fields. ....	28
Table 3.1. Magnetic properties of nanoparticles. ....	51
Table 3.2 Parameters for mathematical model.....	53
Table 3.3. Comparison of alignment times at constant magnetic field for different viscosities of epoxy for GNP and Fe <sub>3</sub> O <sub>4</sub> -GNP nanoparticles.....	60
Table 4.1. Roughness parameters of fractured surfaces for nanocomposites .....	90
Table 4.2. Magnetic properties of nanoparticles. ....	90
Table 5.1. The sample designation and mechanical properties of nanocomposites with GNP and aligned Fe <sub>3</sub> O <sub>4</sub> -GNP nanoparticles. ....	128
Table 5.2: The sample designation and roughness parameters of fractured surfaces for nanocomposites with GNP and aligned Fe <sub>3</sub> O <sub>4</sub> -GNP nanoparticle.....	128
Table 6.1. The fatigue crack growth characteristics of epoxy, GNP epoxy, and aligned Fe <sub>3</sub> O <sub>4</sub> - GNP epoxy nanocomposites .....	157
Table 6.2. The roughness parameters of fractured surfaces by Fatigue Crack Growth in epoxy, GNP epoxy, and aligned Fe <sub>3</sub> O <sub>4</sub> -GNP epoxy nanocomposites .....	163
Table 7.1. Summary of all parameters used in the present study.....	198
Table 7.2. Comparison of the present study results with experimental and analytical predictions found in the literature .....	198

## List of Abbreviations

<b>Abbreviation</b>	<b>Definition</b>
AC	Alternating Current
AFM	Atomic Force Microscopy
ASTM	American Society for Testing and Materials
BADGE	Bisphenol A Diglycidyl Ether
BET	Brunauer–Emmett–Teller
CNF	Carbon Nanofibres
CNT	Carbon Nanotubes
CO	Carbon Monoxide
COD	Crack Opening Displacement
COD <sub>c</sub>	Critical Crack Opening Displacement
CQD	Carbon Quantum Dots
CT	Compact Tension
CTOD	Crack Tip Opening Displacement
CTOD <sub>c</sub>	Critical Crack Tip Opening Displacement
CVD	Chemical Vapor Deposition
DC	Direct Current
DD	Double Distilled
DGEBA	Diglycidyl Ether Bisphenol A
DGEBF	Diglycidyl Ether Of Bisphenol F
DPZ	Debonding Process Zone
DSC	Differential Scanning Calorimetry
EDM	Electrical Discharge Machining
EDS	Energy Dispersion Spectroscopy
EDXMA	Energy-Dispersive X-Ray Microanalysis
FCGR	Fatigue Crack Growth Rate
FRP	Fibre-Reinforced Polymer
FTIR	Fourier-Transform Infrared Spectroscopy
GNP	Graphene Nanoplatelets
GNS	Graphene Nanosheets
HRVM	High-Resolution Video Monitoring
MAP	Magnetophoretic
MWCNT	Multi-Walled Carbon Nanotubes
PE	Polyethylene
PECVD	Plasma-Enhanced Chemical Vapor Deposition
PMMA	Poly Methyl Methacrylate
PVA	Polyvinyl Alcohol
RMS	Root-Mean-Square
RTV	Room Temperature Vulcanization
RVE	Representative Volume Elements
SBR	Styrene Butadiene Rubber
SEM	Scanning Electron Microscopy

SPM	Scanning Probe Microscopy
SWCNT	Single-Walled Carbon Nanotubes
TEM	Transmission Electron Microscopy
TGA	Thermogravimetric Analysis
TGIC	Triglycidyl Isocyanurate
TGMDA	Tetraglycidyl Methylene Dianiline
THF	Tetrahydrofuran
UTM	Universal Testing Machine
VSM	Vibrating Sample Magnetometry
XPS	X-Ray Photoelectron Spectroscopy
XRD	X-Ray Diffraction

## List of Nomenclature

Symbol	Definition
$\bar{m}_{eff}$	effective dipole magnetic moment
$F_m$	attracting magnetic force
$\Omega$	sub-domain $\Omega \rightarrow n$ (=CNT), $i$ (=interphase), $m$ (=matrix)
$a, b$	use as subscript and superscript, $a \rightarrow$ after, $b \rightarrow$ before CNT
$\Delta a$	change in crack length
$C_x, C_y, C_z$	magnetic field components' direction cosines
$A_\Omega, B_\Omega,$	coefficients
$\lambda_\Omega, \mu_\Omega$	Lame constants, shear modulus
$\nu_\Omega$	Poisson's ratio
$\nu_{nc}$	Poisson's ratio of nanocomposite
$v_m$	migration velocity of the nanoparticles
$u, u_{rr, \Omega}$	radial displacements
$\mu_m, \mu_0$	magnetic permeability of epoxy and air
$\xi_a, \zeta_a,$	an assumed factor
$\xi_b, \zeta_b$	
$r, r_n, r_i,$	radii of RVE element, CNT, interphase, matrix, cavity and plastic
$r_m, r_c, r_p$	zone
$L_{xx}, L_{yy}, L_{zz}$	depolarization factor along the respective axis of the ellipsoidal
$l_n$	length of CNT
$V$	volume of RVE
$V_f$	volume fraction of CNT in the RVE
$\hat{V}$	volume of single nanoparticles
$P$	applied load at the outer lateral area of RVE
$H$	global stress concentration tensor (gsct)
$\bar{H}_0$	applied DC magnetic field
$\bar{H}$	induced magnetic intensity within the $Fe_3O_4$ -GNP
$\hat{\sigma}, \hat{\varepsilon}$	stress and strain Field
$\sigma, \varepsilon$	average stress and strain applied at the macro-scale in RVE
$\sigma_{rr}, \varepsilon_{rr}$	mean radial stress and strain
$\sigma_{\theta\theta}, \varepsilon_{\theta\theta}$	mean angular stress and strain
$\bar{\sigma}_p, \bar{\varepsilon}_p$	equivalent plastic stress and strain
$S_{ij}^p, \varepsilon_{ij}^p$	deviatoric stress component of the plastic stress and strain tensor where $(i, j = r, \theta, z)$
$\lambda$	stiffness ratio of interphase and matrix material
$t$	interphase thickness
$t_r$	rotating time
$t_c$	Chaining time
$t_m$	migration time

$t_{s-r}$	<i>slacken rotation time</i>
$t_{s-t}$	<i>slacken translation time</i>
$\bar{T}^m$	<i>magnetic alignment torque</i>
$\bar{T}^H$	<i>hydrodynamic torque</i>
$\lambda_p$	<i>von Mises yield criterion constant</i>
$\delta_{ij}$	<i>Kronecker delta</i>
$\sigma_{kk}$	<i>hydrostatic stress component</i>
$n, n_\Omega$	<i>hardening exponents</i>
$\sigma_Y, \varepsilon_Y$	<i>yield stress and strain</i>
$C_\Omega, D_\Omega$	<i>constant</i>
*	<i>superscript <math>\rightarrow</math> elastic region</i>
$\sigma_{cr}$	<i>critical stress around CNT</i>
$\sigma_{11}, \sigma_{22}, \sigma_{33}$	<i>principal stresses</i>
$\xi_1, \xi_2, \xi_3$	<i>assume constant</i>
$\gamma_i$	<i>interface fracture energy</i>
$K_{I,nc}$	<i>Mode I stress intensity factor of nanocomposite</i>
$K_{IC}, \Delta K_{IC}$	<i>stress intensity factor and range</i>
$\Delta K_{th}, \Delta G_{th}$	<i>Fatigue thresholds</i>
$k_r$	<i>rotational friction coefficient of the particle's geometry</i>
$k_t$	<i>translational friction coefficient</i>
$k_B$	<i>Boltzmann constant</i>
$K_s$	<i>ellipsoidal form factor</i>
$\sigma_n$	<i>average stress at the nano-scale</i>
$\bar{\sigma}_{rr}$	<i>effective radial stress distribution in the DPZ</i>
$G_{IC,nc}, G_{IC,m}$	<i>Mode I critical energy release rate of nanocomposite, neat epoxy and</i>
$\Delta G_i$	<i>contribution of individual toughening mechanism, respectively.</i>
$G_{IC}, \Delta G_{IC}$	<i>strain energy release rate and range</i>
$\Delta G_{cd}, \Delta G_{db},$	<i>Mode I critical energy release rate contribution by crack deflection,</i>
$\Delta G_{pull}, \Delta G_{cv},$	<i>interfacial debonding, CNT pull-out, cavitation, shear band formation</i>
$\Delta G_{SB}, \Delta G_{py}$	<i>and plastic deformation (or yielding) of nanovoids, respectively.</i>
$\phi$	<i>angle with the direction of crack front</i>
$\theta_i, \theta_f$	<i>initial and final angular position of the easy axis</i>
$\theta_{s-r}$	<i>slacken angle</i>
$\rho$	<i>radial distance from the crack tip</i>
$\rho^*$	<i>radius of DPZ at <math>\phi = \pi/2</math></i>
$\eta$	<i>dynamic viscosity of the epoxy</i>
$\Delta U_i, \Delta U_{db},$	<i>Strain energy of individual mechanism, debonding, cavitation and</i>
$\Delta U_{cv}, \Delta U_{py}$	<i>plastic deformation</i>
$U_m$	<i>magnetophoretic mobility of nanoparticles</i>
$w_i, w_{db},$	<i>Strain energy density of individual mechanism, debonding,</i>
	<i>cavitation and plastic deformation</i>

$w_c, w_{py}$	
$\Psi$	<i>a constant factor</i>
$\bar{\chi}_V, \bar{\chi}_{V,yy}, \bar{\chi}_{V,zz}$	<i>tensor magnetic effective volume susceptibility, along x and y axis</i>
$\bar{\chi}_{V,\parallel}, \bar{\chi}_{V,\perp\perp}$	<i>tensor magnetic effective volume susceptibility parallel and perpendicular to the particle's easy axis</i>
$\bar{\chi}_{V,a}$	<i>volume anisotropic susceptibility</i>
$x,y,z$	<i>Axis</i>
$\Theta$	<i>an assumed factor</i>

## Preface

---

---

Researchers are exploring emerging materials to enhance engineering systems by improving performance, reducing components, minimizing maintenance, achieving weight reduction, enhancing corrosion resistance, increasing design flexibility, improving fatigue resistance, leveraging thermal and electrical properties, enhancing impact resistance, achieving cost-effectiveness, ensuring biocompatibility, and enhancing reliability. Composites combine distinct phases to retain individual qualities while exhibiting superior properties. Nanocomposites are a specific focus in this thesis on materials.

Chapter 1 lays the groundwork for GNP epoxy nanocomposites research. It explores the basics of nanocomposites, their applications, and the objective of developing a GNP epoxy nanocomposite. The chapter outlines the research aims, such as characterizing mechanical properties and exploring potential applications. It also emphasizes that this study serves as a basis for future research, providing a starting point for advancements in nanocomposites and expanding scientific knowledge.

Chapter 2 provides a detailed analysis of carbon nanomaterials epoxy composites. It includes an overview of epoxy, its classification, and structure. The chapter explores various studies on the use of nanomaterials for nonreinforcement purposes, with a focus on GNP and carbon nanotubes (CNT). The properties, applications, fabrication process, and real-world implementation of nanocomposites are extensively examined in this chapter.

Chapter 3 focuses on developing a mathematical model to understand the alignment mechanisms of GNP and  $\text{Fe}_3\text{O}_4$ -GNP in an epoxy matrix under a magnetic field. The model considers rotational, translational, chaining, migration, and slackening motions. Key alignment parameters, such as magnetic field strength and epoxy viscosity, are optimized to achieve a fully

cured nanocomposite with aligned Fe<sub>3</sub>O<sub>4</sub>-GNP particles. Surprisingly, a weaker magnetic field is found to be sufficient for aligning Fe<sub>3</sub>O<sub>4</sub>-GNP, unlike GNP, revealing interesting alignment requirements.

Chapter 4 focuses on the synthesis of Fe<sub>3</sub>O<sub>4</sub>-GNP nanoparticles by attaching Fe<sub>3</sub>O<sub>4</sub> to GNP surfaces. The nanoparticles are extensively characterized using techniques such as XRD, FTIR, Raman spectroscopy, TGA, DSC, AFM, XPS, BET, TEM, SEM, EDXMA, and VSM. Aligned Fe<sub>3</sub>O<sub>4</sub>-GNP nanocomposites are successfully fabricated by optimizing parameters, and their alignment within the epoxy matrix is confirmed through characterization methods, optical microscopy, and fracture surface analysis. The investigation validates the suitability of these nanocomposites for various applications.

Chapter 5 focuses on evaluating the implications of incorporating aligned Fe<sub>3</sub>O<sub>4</sub>-GNP epoxy nanocomposites. The study analyzes key parameters such as crack growth resistance,  $K_{IC}$ ,  $G_{IC}$ ,  $CTOD_c$ , and fracture mechanisms, comparing them with GNP nanocomposites. Through optical and AFM imaging techniques, the investigation provides valuable insights into fracture toughness mechanisms, showcasing the significant potential of aligned Fe<sub>3</sub>O<sub>4</sub>-GNP reinforced nanocomposites in various engineering applications.

Chapter 6 extensively investigates the fatigue thresholds ( $\Delta K_{th}$  and  $\Delta G_{th}$ ) and fatigue crack growth rate (FCGR) resistance of GNP and aligned Fe<sub>3</sub>O<sub>4</sub>-GNP nanocomposites. The incorporation of these additives has shown remarkable improvements in mitigating fatigue crack growth and enhancing overall fatigue lifespan of the epoxy material. Aligned Fe<sub>3</sub>O<sub>4</sub>-GNP nanoparticles exhibit exceptional fatigue properties, surpassing those of GNP nanocomposites. This finding underscores the significant potential of aligned Fe<sub>3</sub>O<sub>4</sub>-GNP nanocomposites in applications requiring superior fatigue resistance.

In Chapter 7, a comprehensive multi-scale and multi-mechanism mathematical framework for CNT/epoxy nanocomposites' fracture characteristics is presented. The model incorporates multiple scales and mechanisms, including debonding, cavitation, and plastic deformation of nanovoids. It predicts enhanced fracture energy and shows good agreement with experimental and analytical results. The model's performance is encouraging, demonstrating qualitative agreement with existing literature data.

Chapter 8 concludes the research with a comprehensive summary of the findings and recommendations for future work. It consolidates the key conclusions and proposes avenues for further exploration and advancement in the field, serving as a guide for future investigations.

The chapters enhance the understanding and optimization of nanocomposites, emphasizing aligned  $\text{Fe}_3\text{O}_4$ -GNP reinforced materials for advanced engineering applications. The exploration of fracture characteristics, including a mathematical model for CNT/epoxy nanocomposites, provides valuable insights and accurate predictions for fracture behavior.